

Structure and Electrical Properties of $(\text{Mg}/\text{ZrO}_2)_{52}$ Multilayer Nanostructures

O. V. Stognei^{a, *}, A. N. Smirnov^a, A. V. Sitnikov^a, and M. N. Volochaev^b

^a Voronezh State Technical University, Voronezh, 394006 Russia

^b Kirensky Institute of Physics, Siberian Branch, Russian Academy of Sciences, Krasnoyarsk, 660036 Russia

*e-mail: sto.sci.vrn@gmail.com

Received April 14, 2023; revised May 15, 2023; accepted May 29, 2023

Abstract— $(\text{Mg}/\text{ZrO}_2)_{52}$ multilayer nanostructures with different thicknesses of Mg layers and the same thickness of ZrO_2 layers are obtained via the ion-beam sputtering of two targets in an argon medium. The thickness of one bilayer ($\text{Mg} + \text{ZrO}_2$) varies from 3.6 to 8.5 nm. It is found that using zirconium dioxide prevents the oxidation of the magnesium phase. An electric percolation threshold is observed when the morphology of magnesium layers changes (a transition from discrete to continuous morphology) as a result of an increase in the bilayer thickness. A change of the electrotransport mechanism is identified in the $(\text{Mg}/\text{ZrO}_2)_{52}$ multilayer nanostructures upon passing through the percolation threshold.

DOI: 10.3103/S1062873823703343

INTRODUCTION

Hydrogen energy remains one of the main alternatives in energy development, despite the number of technical problems that limit its commercial scope. One problem is creating a reliable way of safely storing hydrogen in the form of metal hydrides [1]. A solution to this problem using nanostructured materials based on magnesium (a light element that ensures a high mass fraction of adsorbed hydrogen in a material) [2]. Promising materials are multilayer nanostructures in which magnesium layers are interspersed with layers of a dielectric catalyst (e.g., Mg/NbO systems) [3, 4]. Being a chemically active element, magnesium is unfortunately oxidized during the formation of a multilayer structure, even though it and niobium oxide are deposited in sequence, rather than simultaneously [3, 4]. The thinner the magnesium layers (which is desirable for improving the kinetics of hydrogen adsorption/desorption), the stronger the effect its oxidation has on a material's structural properties. The aim of this work was to study the possibility of obtaining a multilayer nanostructure with unoxidized magnesium using chemically stable zirconium oxide. Our objects of study were obtained in a unique way that allowed us to change the thickness of magnesium layers smoothly, since the optimum structure for the formation of hydride is one with multiple discrete layers of magnesium (i.e., layers representing nanoscale magnesium particles that do not contact each other).

EXPERIMENTAL

$(\text{Mg}/\text{ZrO}_2)_{52}$ multilayer nanostructures (where 52 is the number of bilayers) were obtained via the ion-beam sputtering of two targets, one metallic (Mg) and one dielectric (ZrO_2). The sputtered materials were deposited in succession onto substrates moving in a circle around the targets positioned in the central part of the vacuum chamber. Magnesium layers were deposited through a screen with a V-shaped cut. The screen was placed between the target and substrate holder, allowing us to form layers of magnesium with different thicknesses in the same process of deposition. The thickness of the magnesium layers in each sample was determined by its position relative to the screen with the V-shaped window. Samples positioned opposite the narrow part of the V-shaped cut in the screen had the minimum thickness of the magnesium layers. Samples positioned opposite the wide part of the window had the maximum thickness of the magnesium layers. Layers of zirconium oxide were sputtered without the screen, so their thickness was the same in all samples. Substrates made 52 revolutions around the targets throughout the deposition process, so the final samples had 52 bilayers ($\text{Mg} + \text{ZrO}_2$). Our study used samples taken from substrates of three types: glass ceramics, cover glass, and single-crystal silicon. The samples on glass ceramic substrates were used to study the electrical properties of the obtained multilayer nanostructures; those on glass substrates were used for X-ray diffraction studies (total diffraction); and those on single-crystal silicon substrates were intended for small-angle X-ray reflectometry.

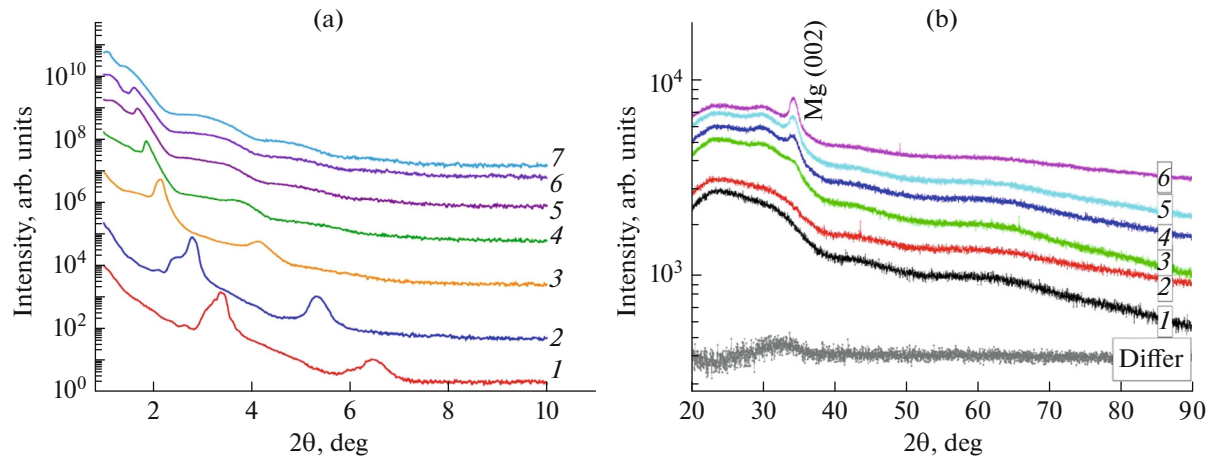


Fig. 1. Data from the X-ray diffraction of samples of a $(\text{Mg}/\text{ZrO}_2)_{52}$ multilayer structure with different thicknesses of one bilayer. (a) X-ray small-angle reflectometry: (1) 3.8; (2) 4.6; (3) 5.9; (4) 6.4; (5) 7.1; (6) 7.7; and (7) 8.4 nm. (b) Total X-ray diffraction: (1) 4.2; (2) 4.9; (3) 6.2; (4) 7.4; (5) 8; and (6) 8.5 nm. The “Differ” curve shows the difference between curve 1 and the background from a clean glass substrate.

Prior to sputtering, the chamber was evacuated to a pressure of 10^{-6} Torr with oil-free pumping. It was then brought to a working pressure of 8.2×10^{-4} Torr with a subsequent injection of Ar (99.9995). The structure of the resulting samples was studied via X-ray diffraction analysis on a D2 Phazer diffractometer using Bragg–Brentano geometry and a wavelength of 0.1541 nm, and by high-resolution transmission electron microscopy on a Hitachi HT7700 microscope. Samples on glass ceramic substrates were thinned by an ion beam (FIB, Hitachi FB2100). The electrical properties of multilayer samples were studied via two-probe potentiometry. Probes were placed on the upper surface of each multilayer structure and the electric current was oriented along its layers. The temperature dependences of the electrical resistance of the samples in the range of 77–273 K were measured inside a continuous-flow nitrogen cryostat.

RESULTS AND DISCUSSION

The multilayered structure of our samples was confirmed by a set of experimental data, primarily from small-angle X-ray reflectometry. Figure 1a presents results from small-angle X-ray reflectometry of multilayer nanostructure samples $(\text{Mg}/\text{ZrO}_2)_{52}$ with different thicknesses of one bilayer ($\text{Mg} + \text{ZrO}_2$). These dependences are characteristic of multilayer nanostructures [5]. The shift of the peaks to the region of small angles corresponds to the increase in the thickness of one bilayer as a result of an increase in the thickness of the magnesium layer.

The thickness of the bilayers in the obtained multilayer structure was estimated in two ways. We first used small-angle reflectometry data (Fig. 1a), where the angular position of the maximum on the reflecto-

gram allows us to estimate the period of the multilayered structure via X-ray refraction. Period D of modulation can be determined as

$$D = \frac{n\lambda}{2 \sin \theta}, \quad (1)$$

where λ is the wavelength of the radiation; n is the order of reflection; and θ is the angle of the observed maximum.

Results for ten samples were approximated by a polynomial, allowing us to determine the thickness of one bilayer for each sample.

The thickness of one bilayer was then estimated on the basis of data from scanning electron microscopy, allowing us to determine the thickness of an entire multilayer sample. Dividing this value by the number of layers (or the number of revolutions made by the substrate holder around the targets during sputtering) gave the thickness of one bilayer. The difference between the values of bilayer thickness determined in different ways was 15%, but it allowed us to operate with the resulting values in analyzing the electrical properties of multilayer samples. According to our estimate, the nominal thickness of a bilayer ($\text{Mg} + \text{ZrO}_2$) varied in the range of 3.5–8.5 nm.

Additional confirmation that the obtained samples were really multilayer specimens was a microphotograph of the cross section of a multilayer $(\text{Mg}/\text{ZrO}_2)_{52}$ sample with a calculated bilayer thickness of 8 nm. Data based on high-resolution transmission electron microscopy (Fig. 2) also indicated that the thickness of one bilayer was estimated correctly.

Figure 1b shows X-ray diffractograms of $(\text{Mg}/\text{ZrO}_2)_{52}$ multilayer samples sputtered onto glass substrates in the initial state. The obtained diffractograms can be divided into two groups. The first group

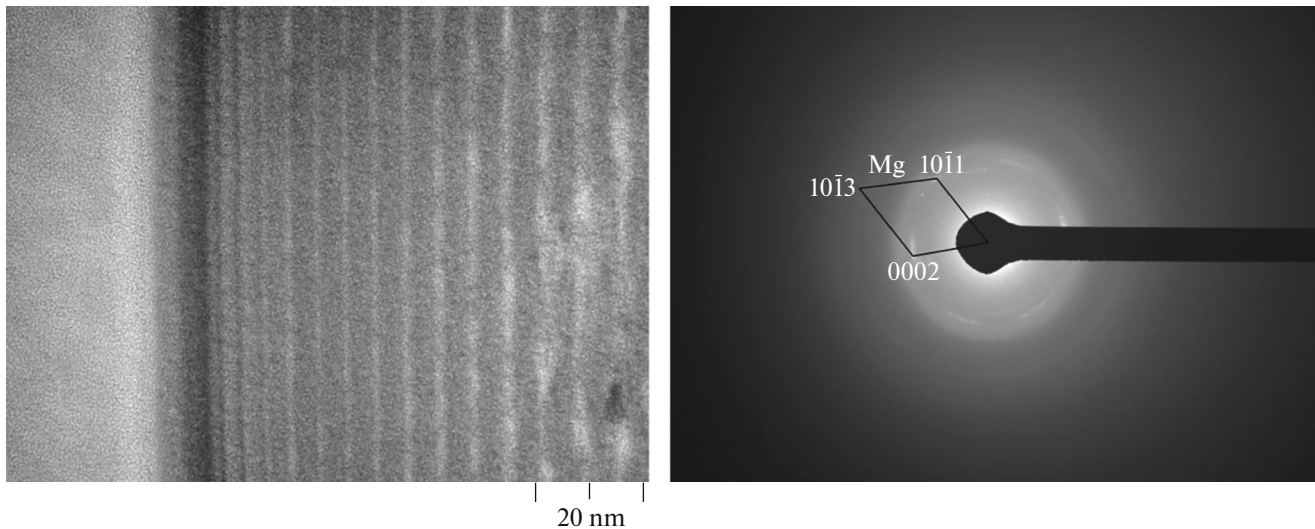


Fig. 2. Micrograph of the cross section and electron diffraction of the $(\text{Mg}/\text{ZrO}_2)_{52}$ multilayer sample with a calculated bilayer thickness of 8 nm.

contains X-ray diffractograms with no peaks; the second, X-ray diffractograms with one peak.

The first group (Fig. 1b, curves 1 and 2) is characterized by a broad halo that is a superpositioning of two halos. One halo ($20\text{--}28^\circ$) corresponds to a glass substrate; the other halo ($28\text{--}34^\circ$), to the amorphous phase of zirconium oxide. Figure 1b contains a curve labeled Differ, which is the difference between the intensity of radiation reflected from sample 1 (on a glass substrate) and radiation reflected from a clean glass substrate (actually the signal from the sample minus the one from the substrate). It is obvious that there is a single halo in the range of angles corresponding to the angular position of the (111) peak in crystalline zirconium oxide.

Films of pure unstabilized zirconium oxide obtained via the ion-beam sputtering of ceramic targets usually form with a nonequilibrium orthorhombic structure [6–8]. If zirconium oxide contains any stabilizing additives (most often yttrium), a monoclinic, tetragonal, or cubic modification forms, depending on the amount of the additive [9, 10]. No diffraction peaks from crystalline zirconium oxide were observed in our sputtered $(\text{Mg}/\text{ZrO}_2)_{52}$ multilayer nanostructures. Neither did the electron diffractogram obtained from a sample with a bilayer thickness of 8 nm show any reflections from crystalline zirconium oxide (see Fig. 2). This indicates zirconium oxide proved to be amorphous rather than crystalline in the multilayer structure that formed as a result of sputtering. The existence of an amorphous structure in sputtered films of zirconium dioxide has been confirmed [11]. Effectively removing heat from a sputtered film is enough to form a disordered structure in zirconium dioxide. In our case, dioxide sputtering onto the rotating substrate

apparently created sufficient conditions for the formation of an amorphous structure. The duration of the direct deposition of dioxide atoms (oxygen and zirconium) that brought energy to the substrate was fairly short (until the substrate was in the target sputtering zone, i.e., around 52 s), while the complete rotation of the substrate inside the chamber lasted 420 s. The dioxide structure formed on a surface of a metal (magnesium) with high thermal conductivity, ensuring the rapid removal of heat. No diffraction peaks from the magnesium phase were observed in the samples of this group, due to the thinness of the metal interlayers.

In addition to the halo from zirconium oxide, the diffractograms of the second group (Fig. 1b, curves 3–6) contained a peak with an angular position corresponding to 34 degrees. It is difficult to attribute this peak to any phase, but based on the elemental composition of the samples and how they were sputtered, it is logical to assume the observed peak resulted from reflections off the (002) crystallographic planes of magnesium. This assumption is supported first of all by magnesium being an element with a hexagonal lattice. The sputtering of thin films of metals with hexagonal structure usually results in texturization that suppresses reflections from some planes and enhances X-rays reflected from other planes. The texturization of magnesium films obtained via sputtering is seen fairly often in experiments. It has been observed in sputtered thin films of pure magnesium [12], Mg/NbO multilayer structures [3, 4], films of MgNi alloys [13], and films of Pd or La solid solutions based on magnesium [14, 15]. In all cases, a strong increase in reflections from the family of (002) planes and almost complete suppression of other reflections were recorded. The (002) reflection in magnesium should be observed at precisely $2\theta = 34^\circ$. Second, the diffractograms

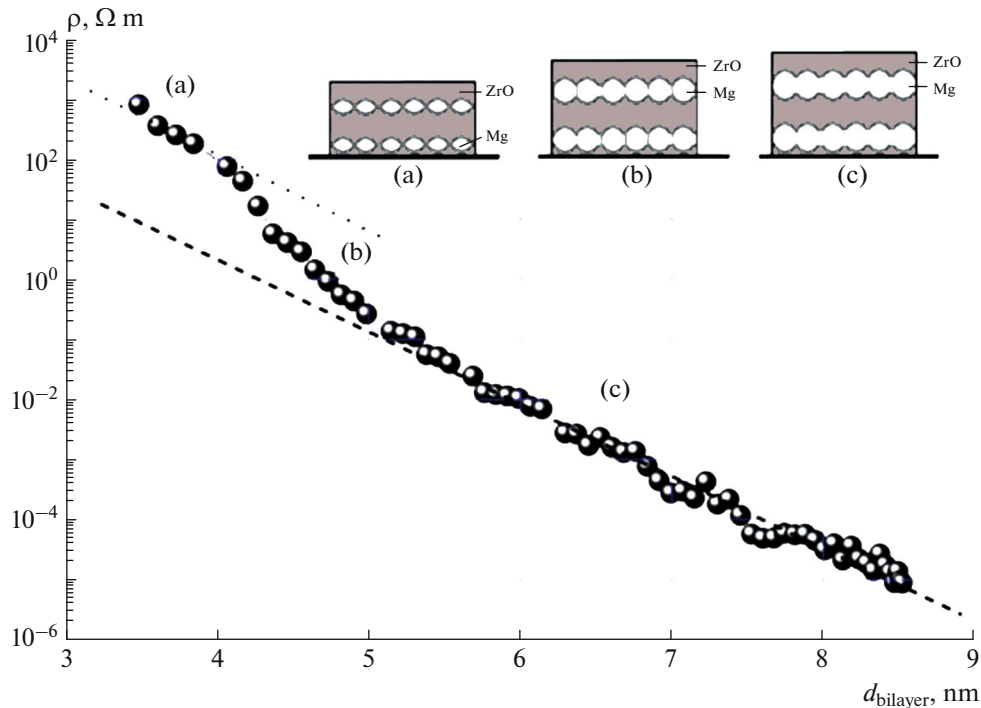


Fig. 3. Dependence of the specific resistance of samples of a $(\text{Mg}/\text{ZrO}_2)_{52}$ multilayer nanostructure on the thickness of one bilayer. The inset shows a diagram of the structure of (Mg/ZrO_2) multilayer samples: (a) separate nanogranules in the dielectric matrix; (b) magnesium granules merged to form continuous layers with oxide interlayers (percolation threshold); and (c) fully conductive magnesium layers that formed.

(Fig. 1b) show that an increase in the thickness of the bilayer (which results from raising the thickness of magnesium layers) makes the diffraction peak more intense and reduces its width. Third, the electron diffractogram from the $(\text{Mg}/\text{ZrO}_2)_{52}$ sample with a nominal bilayer thickness of 8 nm contains reflections only from metallic magnesium (Fig. 3). These data suggest that the only peak observed in the diffractograms (Fig. 1b) corresponds to reflections from the family of (002) magnesium planes. It is important emphasized there are no other diffraction peaks that could correspond to magnesium oxide on either the diffractograms (Fig. 1) or the electron diffractogram (Fig. 2). Diffraction studies therefore showed there was no oxidation of magnesium layers in our $(\text{Mg}/\text{ZrO}_2)_{52}$ multilayer samples when creating nanostructures via sputtering.

Our study of the electrical properties of $(\text{Mg}/\text{ZrO}_2)_{52}$ multilayer nanostructures, particularly the dependence of the electrical resistance of samples on the thickness of a bilayer (actually on the thickness of magnesium interlayers), and the temperature dependence of the resistance of our samples when heating them from 77 K, suggests that the thickness of magnesium layers had a decisive effect on the morphology.

Figure 3 shows the dependence of the specific resistance of $(\text{Mg}/\text{ZrO}_2)_{52}$ samples on the bilayer

thickness. The form of this dependence is similar to that of the resistance on the concentration of the metal phase in metal–dielectric isotropic nanocomposite media [16]. There are two almost linear regions with high and low resistance, separated by a transitional region. The region of high resistance corresponds to composites in which the metal phase is nanogranules isolated from one another in the dielectric matrix. The state of low resistance is characteristic of composites with a metal matrix in which nanoscale dielectric regions are distributed. The transitional region in the nanocomposites corresponds to the percolation threshold (i.e., to the concentration of the metal phase at which a percolation cluster forms as a result of the fusion of separate metal granules into conducting chains). We believe a similar situation occurs in the magnesium layers of $(\text{Mg}/\text{ZrO}_2)_{52}$ multilayer samples upon an increase in the thickness of the metal layers.

At one bilayer thicknesses of 3.4 to 4 nm, the magnesium layers are discrete (formed from separate nanoscale granules) rather than continuous. This is confirmed by the high specific resistance of our samples (10^2 – 10^3 Ohm m) and the form of the temperature dependence of the electrical resistance of samples of this group (Fig. 4). Figure 4 shows dependences that were measured while heating of the samples from 77 to 273 K. The changes in resistance in this range of temperatures were determined only by features of the elec-

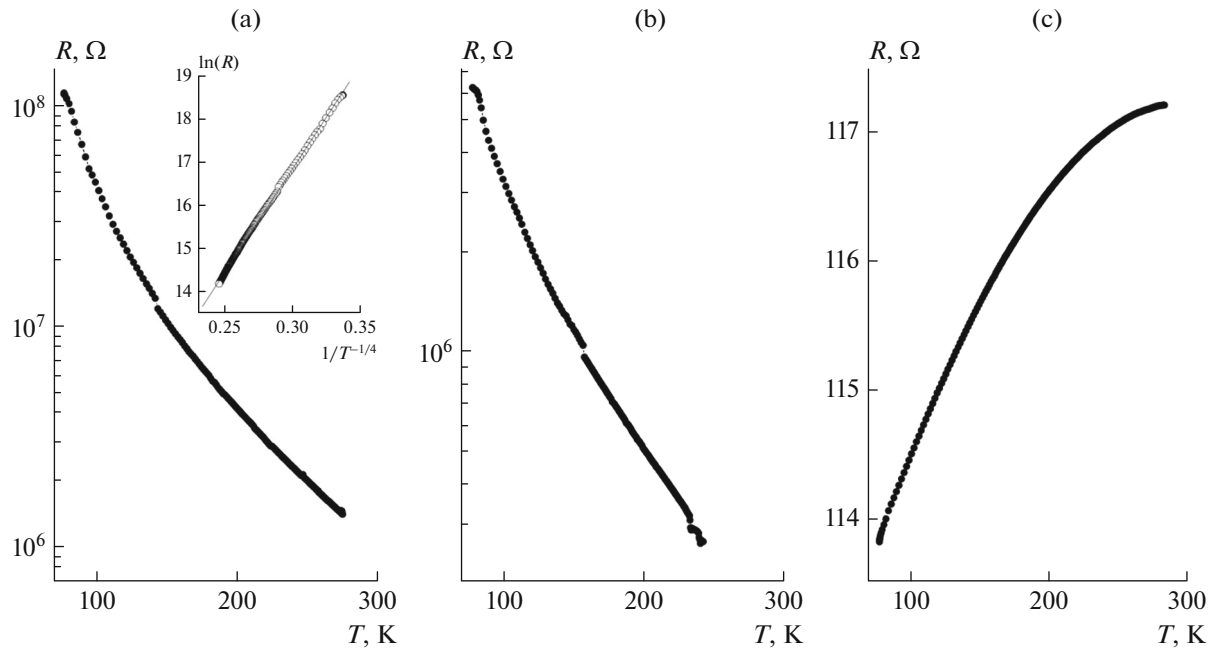


Fig. 4. Temperature dependence of the resistance of samples of a $(\text{Mg}/\text{ZrO}_2)_{52}$ multilayer nanostructure for different thicknesses of its magnesium layers: (a) 3.6; (b) 4.4; and (c) 5.9 nm.

transport mechanism in the material, since possible relaxation processes took place when the samples were naturally exposed to room temperature. The temperature dependence of the resistance in the multilayer sample with a single bilayer thickness of 3.6 nm (Fig. 4a) was obviously thermally activated rather than metallic. Analysis of the temperature dependence of the resistance in the Mott model for hopping conductivity with variable hop length [17] confirmed that magnesium layers are not continuous at thicknesses of 3.6–4 nm. This conductivity is due to the tunneling of electrons through localized states in the band gap of a semiconductor or a dielectric with energies close to the Fermi level. This mechanism of conduction should produce an exponential dependence of the resistance on temperature: $R = R_0 \exp[(T/T_0)^{-1/4}]$. The inset in Fig. 4a shows the experimental dependence rearranged in coordinates of the Mott model ($\ln R$ on $T^{-1/4}$). The dependence is obviously linearized in these coordinates, confirming the hopping mechanism of transport. In other words, there were no channels with metallic conductivity in the samples of this group, and the charge was transported along defects of the dielectric phase. Inset (a) in Fig. 3 shows the hypothetical morphology of $(\text{Mg}/\text{ZrO}_2)_{52}$ samples with minimum bilayer thickness. We should emphasize that despite there being no diffraction peaks from magnesium in the X-ray diffractograms (curves 1 and 2, Fig. 1b), magnesium formed a discrete layer with a pronounced interface, rather than being dissolved in the zirconium dioxide. Otherwise, there would be no peaks in the low-angle reflectograms (Fig. 1a).

The transport mechanism changed fundamentally at bilayer thicknesses greater than 5 nm, and we observed a positive temperature coefficient of resistance that was characteristic of metallic conductivity (Fig. 4c). This suggests that magnesium forms continuous metal layers at such thicknesses, allowing charge transport along them. Inset (c) in Fig. 3 shows the hypothetical morphology of samples with continuous magnesium layers. The existence of continuous layers of magnesium in multilayer samples with bilayer thicknesses of more than 5 nm was confirmed by a micrograph of the cross section (Fig. 2, light regions).

The intermediate range of bilayer thicknesses (4–5 nm) corresponds to the electrical percolation threshold (i.e., the thickness at which separate magnesium particles begin to merge with one another in a single layer, thereby forming percolation clusters). In this range of values, the change in the resistance of the multilayer structure upon an increase in thickness was sharper than those in linear regions. The specific resistance in this case fell by three orders of magnitude when the bilayer thickness was raised by 1 nm (Fig. 3), in contrast to regions (a) and (b).

CONCLUSIONS

Successive sputtering of magnesium and zirconium dioxide in an argon medium (8.2×10^{-4} Torr) yielded multilayer nanostructure $(\text{Mg}/\text{ZrO}_2)_{52}$ with unoxidized magnesium layers of nanoscale thickness.

Placing a screen with a V-shaped window between the sputtered magnesium target and substrates allowed

us to sputter the $(\text{Mg}/\text{ZrO}_2)_{52}$ multilayer nanostructure with a gradient of magnesium layer thickness and a constant zirconium dioxide layer thickness. The thickness of one $(\text{Mg} + \text{ZrO}_2)$ bilayer in the resulting multilayer samples varied from 3.5 to 8.5 nm.

The morphology of magnesium layers was determined from their thickness. We found that magnesium layers were discrete in thin $(\text{Mg} + \text{ZrO}_2)$ bilayers (3.5–4 nm). The existence of an electric percolation threshold was established in the $(\text{Mg}/\text{ZrO}_2)_{52}$ multilayer structure. The threshold corresponded to a change in the morphology of magnesium layers, from discrete to continuous.

FUNDING

This work was supported by the RF Ministry of Science and Higher Education as part of a State Task, project no. FZGM-2023-0006; and as part of project no. 075-15-2021-709 (unique identifier RF-2296.61321X0037; control measurements).

CONFLICT OF INTEREST

The authors declare that they have no conflicts of interest.

REFERENCES

- Murray, P., Orehounig, D., Grosspietsch, K., and Carmeliet, J., *Appl. Energy*, 2018, vol. 231, p. 1285.
- Lin, X., Zhu, Q., Leng, H., et al., *Appl. Energy*, 2019, vol. 250, p. 1065.
- Stognei, O.V., Smirnov, A.N., Sitnikov, A.V., and Semenenko, K.I., *Solid State Commun.*, 2021, vol. 330, p. 114251.
- Liu, J., Fu, Y., Huang, W., *J. Phys. Chem. C*, 2020, vol. 124, p. 6571.
- Zubarev, E.N., *Phys.—Usp.*, 2011, vol. 54, no. 5, p. 473.
- Sponchia, G., et al., *J. Eur. Ceram. Soc.*, 2017, vol. 37, p. 3393.
- Francisco, L., Sponchia, G., Benedetti, A., et al., *Ceram. Int.*, 2018, vol. 44, no. 9, p. 10362.
- Trolliard, G., Benmechta, R., and Mercurio, D., *Acta Mater.*, 2007, vol. 55, p. 6011.
- Golovin, Yu.I., *Keramicheskie materialy na osnove dioksida tsirkoniya* (Ceramic Materials Based on Zirconia), Moscow: Tekhnosfera, 2018.
- Thornton, J.A., *J. Vac. Sci. Technol., A*, 1986, vol. 6, no. 4, p. 3059.
- Ceresoli, D. and Vanderbilt, D., *Phys. Rev. B*, 2006, vol. 74, p. 125108.
- Platzer-Björkman, C., Mongstad, T., Karazhanov, S., et al., *Mater. Res. Soc. Symp. Proc.*, 2009, vol. 1210, p. 315.
- Ouyang, L.Z., Ye, S.Y., Dong, H.W., and Zhu, M., *Appl. Phys. Lett.*, 2007, vol. 90, p. 021917.
- Ouyang, L., Qin, F.X., Zhu, M., et al., *J. Appl. Phys.*, 2008, vol. 104, p. 016110.
- Pasturel, M., Slaman, M., Schreuders, H., et al., *J. Appl. Phys.*, 2006, vol. 100, p. 023515.
- Gridnev, S.A., Kalinin, Yu.E., Sitnikov, A.V., and Stognei, O.V., *Nelineinye yavleniya v nano- i mikrogeterogennykh sistemakh* (Nonlinear Phenomena in Nano- and Microheterogeneous Systems), Moscow: BINOM. Laboratoriya Znaniy, 2012.
- Mott, N.F. and Davis, E.A., *Electron Processes in Non-Crystalline Materials*, Oxford: Clarendon, 1979, vol. 1.

Translated by D. Zabolotny